

## Structures of Oxide Nanobelts and Nanowires

Z.L. Wang,\* Z.W. Pan, and Z.R. Dai

Center for Nanoscience and Nanotechnology, School of Materials Science and Engineering, Georgia Institute of Technology, Atlanta, GA 30332-0245, USA

**Abstract:** We have recently reported the synthesis of one-dimensional nanobelt structures of ZnO, SnO<sub>2</sub>, In<sub>2</sub>O<sub>3</sub>, CdO, Ga<sub>2</sub>O<sub>3</sub>, and PbO<sub>2</sub> by evaporating the desired commercial metal oxide powders at high temperatures (*Science* (2001), **291**, 1947). The as-synthesized oxide nanobelts are pure, structurally uniform, single crystalline, and most of them free from dislocations. The beltlike morphology appears to be a unique and common structural characteristic for the family of semiconducting oxides. In the present article, we focus on the twin and stacking fault planar defects found in oxide nanobelts and nanowires although they are rarely observed. Some interesting and unique growth morphologies are presented to illustrate the roles played by surface energy and kinetics in growth. It is shown that the surfaces of the oxide nanobelts are enclosed by the low-index, low-energy crystallographic facets. The growth morphology is largely dominated by the growth kinetics.

**Key words:** oxide nanobelts, oxide nanowires, ZnO, SnO<sub>2</sub>, In<sub>2</sub>O<sub>3</sub>, CdO

### INTRODUCTION

One-dimensional quantum wires are of fundamental importance to the study of size-dependent chemical and physical phenomena. With a decrease in sizes, unique electrical, mechanical, chemical, and optical properties are introduced, which are largely believed to be the result of surface and/or quantum confinement effects. The most important challenges for future nanoelectronics are interconnects and the integration among interconnects and devices. Nanowire-like structures are ideal systems for studying the transport process in one-dimensional objects, which are potential candidates for understanding the quantum phenomena in the interconnects. As the sizes of the devices shrink below 100 nm, searching and building three-dimensional interconnects is the key for nanoelectronics. It is natural to explore

the possibility of building functional devices in the wires, so that the interconnects and devices are conjunctive, self-integrated, and inseparable.

Much of the study of one-dimensional structures has been focused on carbon nanotubes (Iijima, 1991), silicon nanowires, and compound semiconductor nanowires (Morales and Lieber, 1998), such as InP. Our research has been focused on nanostructures of functional oxides. Some of the transition and rare earth metal oxides are semiconducting, and they are fundamental to the development of smart and function devices, which have key applications in electromechanical, electrooptical, electrochemical, and optothermal applications (Wang and Kang, 1998). The metal oxides will have two important characteristics, including (1) cations with mixed valences, and (2) significant oxygen vacancies. The oxides are usually made into single crystals, dispersive nanoparticles, or condensed films. Recently, we have synthesized ultralong beltlike nanostructures of semiconducting oxides of zinc, tin, indium, cadmium, and gal-

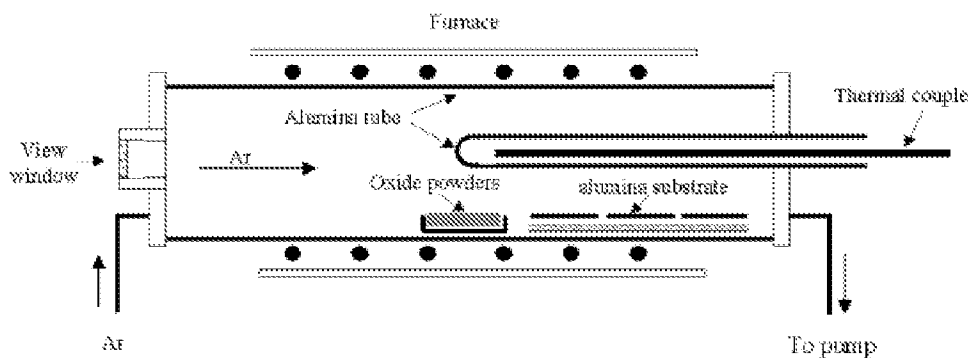


**Figure 1.** Experimental setup for the synthesis of nanobelt structures.

lium, by simply evaporating the desired commercial metal oxide powders at high temperatures (Dai et al., 2001b; Pan et al., 2001b). The as-synthesized oxide nanobelts are pure, structurally uniform, and single crystalline, and most of them free from dislocations. They have a rectangular-like cross section with typical widths of 30 to 300 nm, width-to-thickness ratios of 5 to 10 and lengths of up to a few millimeters.

In this article, we focus on the planar defects found in the oxide nanobelts, although they are rarely observed. A variety of unique structures are shown to demonstrate that the morphology of the nanobelts is governed not only by surface energy but also by growth kinetics.

## SYNTHESIS METHOD

Our synthesis is based on thermal evaporation of oxide powders under controlled conditions without the presence of catalyst (Pan et al., 2001a,b). The desired oxide powders were placed at the center of an alumina tube that was inserted in a horizontal tube furnace (Fig. 1), where the temperature, pressure, and evaporation time were controlled. At one end of the furnace, argon or nitrogen flowed over a crucible containing the raw powder of interest. The temperature distribution inside the tube was measured by a thermocouple, which was inserted inside a thin alumina tube and could be moved freely along the tube axis. During reaction, temperatures at any point between the tube center and the tube's downstream end were monitored *in situ*. Thus, the relationship between the temperature and the growth products was correlated. In our experiments, except for the evaporation temperature that was determined based on the melting point of the oxides to be used, we kept the following parameters constant: evaporation time, 2 h; cham-

ber pressure, 300 Torr; and Ar flowing rate, 50 standard cubic centimeters per minute (sccm). During evaporation, the products were deposited onto an alumina plate placed at the downstream end of the alumina tube.

The as-deposited products were characterized and analyzed by X-ray diffraction (XRD; Philips PW 1800 with Cu K $\alpha$  radiation), scanning electron microscopy (SEM; Hitachi S800 FEG), transmission electron microscopy (TEM; Hitachi HF-2000 FEG at 200 kV and JEOL 4000EX high resolution TEM (HRTEM) at 400 kV), and energy dispersive X-ray spectroscopy (EDS).

## EXPERIMENTAL RESULTS

### Planar Defects in ZnO Nanobelts

Through TEM images, we found that the geometrical shape of the ZnO nanostructures is a belt (Fig. 2). Each nanobelt has a uniform width along its entire length, and the typical widths of the nanobelts are in the range of 50–300 nm. A ripplelike contrast observed in TEM images is due to strain resulting from the bending of the belt. HRTEM and electron diffraction show that the ZnO nanobelts are structurally uniform, single crystalline, and dislocation free. Nanobelts without planar defects grow along [0001] and are enclosed by (2 $\bar{1}\bar{1}0$ ) and (01 $\bar{1}0$ ) facets.

Nanobelts with a single stacking fault are occasionally found, and they grow along [01 $\bar{1}0$ ] and are enclosed by (0001) and (2 $\bar{1}\bar{1}0$ ) facets. The stacking fault is parallel to the axis and runs throughout the entire length of the nanobelt (Fig. 3a). An HRTEM profile image of the nanobelt shows that its surface is clean, atomically sharp, and without a sheathed amorphous layer (Fig. 3b; note that the contrast showing in the image is due to the amorphous carbon film

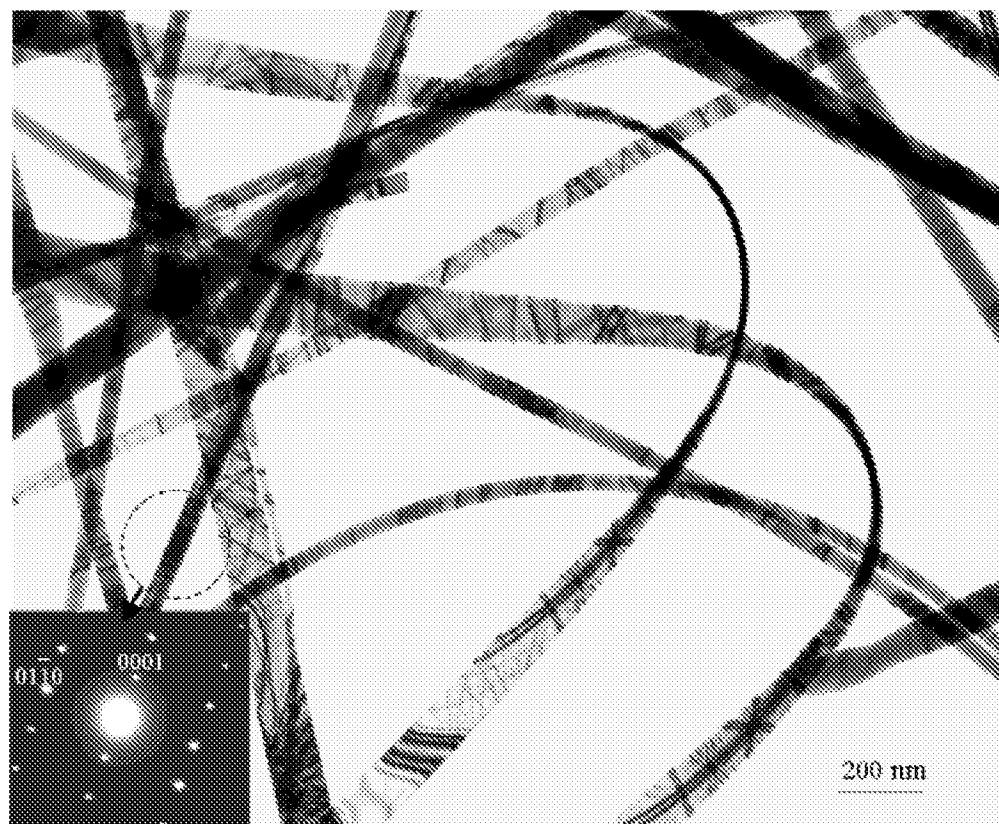


**Figure 2.** Ultralong nanobelt structure of ZnO. The inset is an electron diffraction recorded from the circled area, showing the [0001] growth direction of the nanobelt.

used as a substrate for TEM observation). This is natural because the nanobelts were made at a high temperature and all of the surface steps and defects may be eliminated by annealing. An enlargement of the stacking fault image is given in Figure 3c, and the stacking plane is (0001).

Twin structure is rarely seen in ZnO nanobelts. Shown in Figure 4a is a nanobelt that has a twin structure as proven by the corresponding electron diffraction pattern in Figure 4b. The nanobelt is oriented along  $[2\bar{1}\bar{1}0]$ , the twin plane  $(01\bar{1}\bar{1})$  is parallel to the side surface, and its growth direction  $L$  is perpendicular to the  $(0\ 1\ -1\ 1/3(c/a)^2) = (0\ 1\ -1\ 0.855)$  plane, where  $a$  and  $c$  are the lattice constants for ZnO.

### **In<sub>2</sub>O<sub>3</sub> Nanobelts, Nanosheets, and Nanowires**

Nanobelts of In<sub>2</sub>O<sub>3</sub> were also synthesized by evaporation of In<sub>2</sub>O<sub>3</sub> powders (purity: 99.99%, melting point:  $\sim 1920^\circ\text{C}$ ) at  $1400^\circ\text{C}$  (Fig. 5a). TEM observations show that most of the In<sub>2</sub>O<sub>3</sub> nanobelts have uniform width and thickness along their lengths (Fig. 5b). Typically, the In<sub>2</sub>O<sub>3</sub> nanobelts have

widths in the range of 50 to 150 nm and lengths of several tens to several hundreds of micrometers. In<sub>2</sub>O<sub>3</sub> has the C-rare earth crystal structure (Galasso, 1970), which is a cubic made of 8 CaF<sub>2</sub> units with ordered oxygen vacancies. Electron diffraction (inset in Fig. 5b) analysis shows that the In<sub>2</sub>O<sub>3</sub> nanobelts are single crystalline and grow along  $\langle 100 \rangle$ , and the surfaces are enclosed by  $\{100\}$ , which are apparently the lower energy surface for cubic structures.

From the symmetry point of view, the (100), (010), and (001) surfaces for the cubic system are identical. Therefore, the growth can be either along  $[100]$ ,  $[010]$ , or  $[001]$ ; thus, it is possible to have different growth morphologies. If we only have two possible choices for growth directions such as  $[100]$  and  $[010]$ , we can have the platelet structures as displayed in Figure 6, where most of the facets are (100) and (010), while the (110) type of face is also seen, which is introduced to minimize the surface area, possibly for reducing the total surface energy. These structures have a common characteristic that the surface normal is  $[001]$ , displaying a sheet-type of structure. Electron diffraction from a sheet is given in the inset of Figure 6a. The various shapes shown

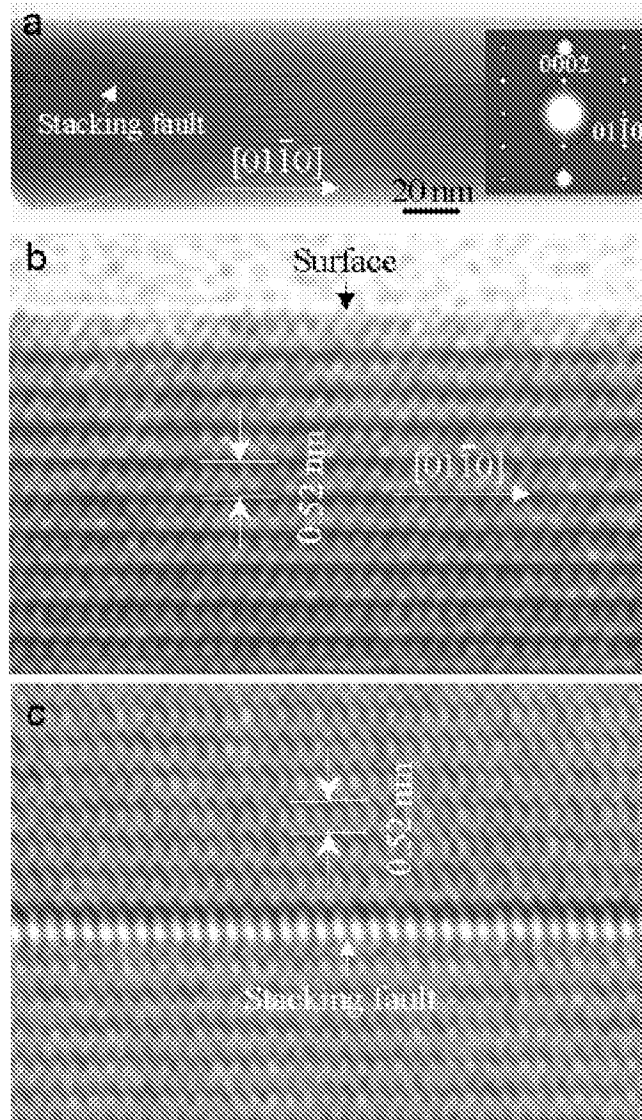


**Figure 3.** **a:** TEM image of a ZnO nanobelt grows along  $[01\bar{1}0]$ , exhibiting a single stacking fault parallel to the growth axis. **b:** High-resolution TEM image from the surface of the nanobelt, showing a clean and atomically flat surface. **c:** High-resolution TEM image from the stacking fault region.

in Figure 6b–e are induced by the  $\{100\}$  and  $\{110\}$  type of facets. These sheets are single crystalline and they have no dislocations and no planar defects. It is interesting to point out that, although the growth along  $[100]$ ,  $[010]$ , and  $[001]$  is equivalent, no cube is found in the growth product.

Twin structure is also found in  $\text{In}_2\text{O}_3$  nanowire (Fig. 7a). The twin is made of two crystals that are joined at a specific angle, as indicated by an enlarged image shown in the inset in Figure 7a. Electron diffraction pattern can be indexed to be  $[11\bar{1}]$  (Fig. 7b), where the dark dashed lines and the

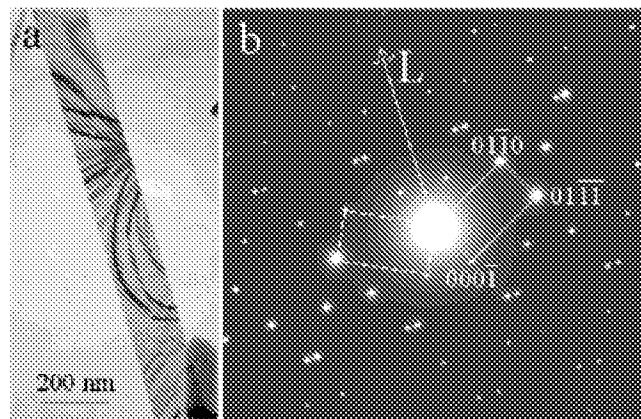


**Figure 4.** **a:** TEM image of a ZnO nanobelt with a twin plane parallel to the growth axis. **b:** The corresponding electron diffraction pattern, beam direction  $[2\bar{1}\bar{1}0]$ .

white dashed lines represent the reflections from the two crystals, and the rotation angle between the two sets of patterns is  $\sim 22^\circ$ . The diffraction pattern is a simple geometrical overlap between two  $[111]$  diffraction patterns that have a  $22^\circ$  relative rotation. The twin plane is  $(123)$  and the wire growth direction is  $[5\bar{4}1]$ . An examination of the image shown in Figure 7a indicates that the side surfaces are made of small facets, which are likely to be the  $\{100\}$  type sawtooth surfaces because of lower surface energy.

If the growths along  $[100]$ ,  $[010]$ , and  $[001]$  are of equal rate, the nanowire takes a form shown in Figure 8a, b. Electron diffraction indicates that the growth direction is  $[111]$ . The structure has numerous  $\{100\}$  facets, but their corners are not as sharp as for a perfect cube due to the high synthesis temperature ( $1400^\circ\text{C}$ ). No dislocations or planar defects were found. The structure is single crystalline and has a “drill” shape, which can be understood from the stacking of cubes, as shown in Figure 8c. The small cubes enclosed by the  $\{100\}$  facets serve as the building blocks; their chain stacking along  $[111]$  would give the wire structure. The sharp corners were truncated due to the sintering at high temperature.

A more complex structure is given in Figure 8d, which grows along  $[111]$ , but which has a superstructure (see the inset electron diffraction pattern). Its diameter is rather large and its surface has a rough morphology.

Nanobelt structures have also been synthesized for  $\text{SnO}_2$  and  $\text{CdO}$  (Pan et al., 2001a,b; Dai et al., 2001a,b),  $\text{Ga}_2\text{O}_3$  (Dai et al., 2001a,b), and  $\text{PbO}_2$  (Pan et al., 2001a,b). Our results show that the beltlike morphology is a genetic and unique structural characteristic for some semiconductive

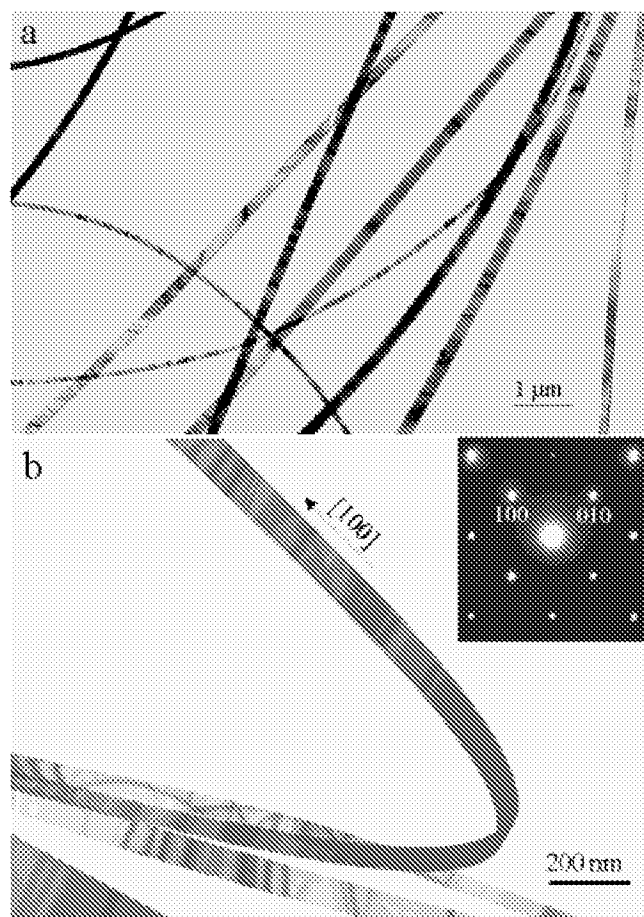


**Figure 5.** TEM images of  $\text{In}_2\text{O}_3$  nanobelts. The inset in **b** is an electron diffraction pattern from the nanobelt, showing its growth direction and side surfaces.

oxides with cations of different valence states and materials belonging to different crystallographic structures. Their structures are well controlled, and the belt shape is defined by some specific crystallographic planes. Table 1 gives a summary on the growth directions and the surface planes of the nanobelts of different materials that we have successfully synthesized. The surfaces of the nanobelts are governed by low index planes, which are likely to be the lower energy surfaces for the crystal structures. The lowest energy surfaces for different types of oxides may be different.  $\text{SnO}_2$  and  $\text{PbO}_2$  both are rutile structures but their nanobelt surfaces are distinctive.

### Growth Kinetics in Controlling the Nanowire Morphology

The morphology of the nanobelts is defined by a combination of surface energy and growth kinetics. Take cubic CdO

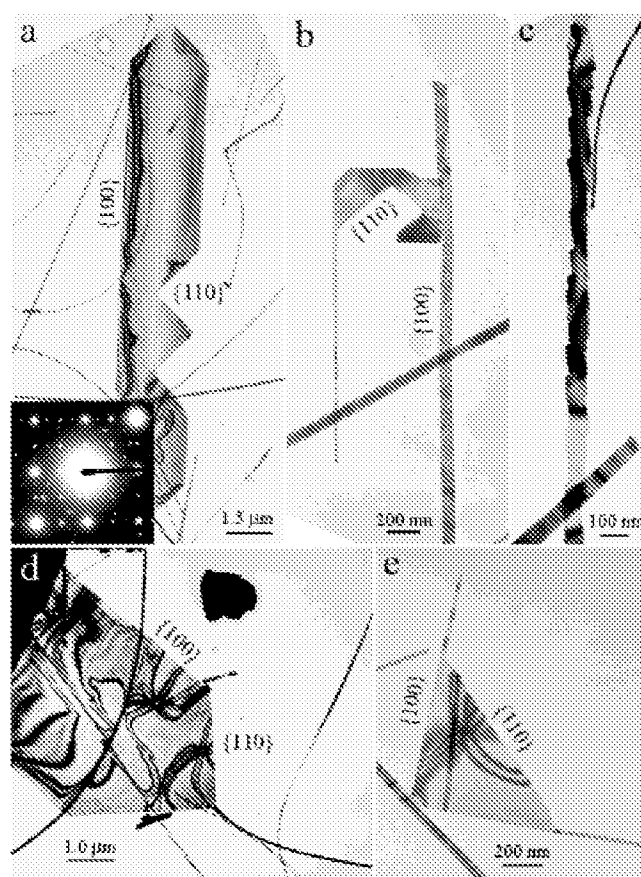


**Figure 6.** Platelet structures of  $\text{In}_2\text{O}_3$  constructed by the low index crystal facets.

as an example; the growth direction can be either  $[100]$  or  $[010]$  because of the isotropic crystal structure, as shown in Figure 9. Many single crystalline CdO sheets with sizes on the order of several to several tens of micrometers were also formed (Fig. 9). CdO has the NaCl cubic structure, and electron diffraction shows that the nanobelts grow along  $[100]$ , and their surfaces are enclosed by  $\pm(001)$  and  $\pm(010)$  facets. The sheet-type of structure is formed due to the equivalent growth rates along  $[001]$  and  $[010]$  (Fig. 9b, d), which are the two fastest growth directions. The image shown in Figure 9a indicates that the growth direction can switch between  $[100]$  and  $[010]$  depending on the growth kinetics. Figure 9c is the result of fast growth along  $[001]$  and  $[010]$ , showing that the growth kinetics determines the morphology.

Figure 10 shows another example of the growth of the single crystalline T-shape  $\text{SnO}_{2-x}$  nanowires. The electron beam direction is  $[101]$ ; the straight nanowire grows perpendicular to the  $(\bar{1}2\bar{1})$  plane, then the growth direction switches to be perpendicular to the  $(\bar{1}21)$  plane. The T-shape resulted

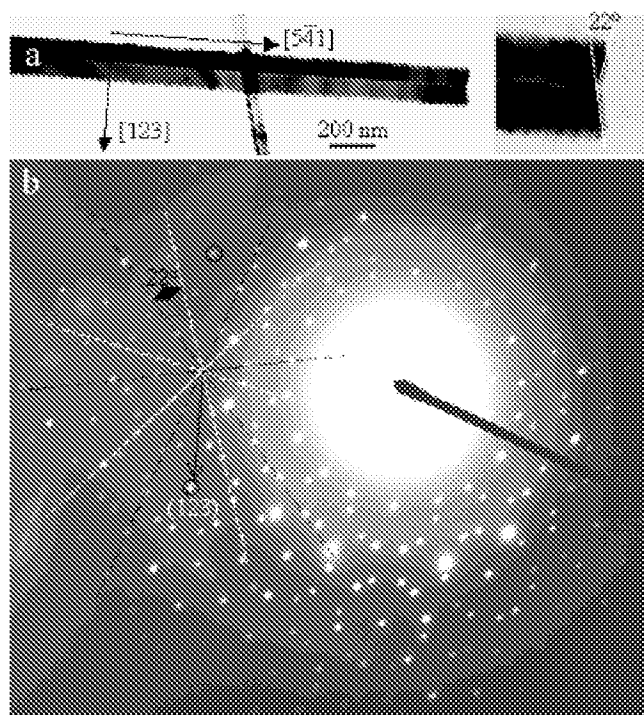


**Figure 7.** **a:** Twin structure observed in  $\text{In}_2\text{O}_3$  and an enlargement of the nanowire. **b:** The corresponding electron diffraction pattern, beam direction  $[11\bar{1}]$

from the growth parallel to  $(1\bar{2}\bar{1})$  and  $(1\bar{2}1)$ , which are two crystallographically equivalent planes. The electron diffraction pattern recorded from the T junction shows its single crystalline structure (Fig. 10b, c). Images recorded from the growth front of the T branch show the absence of a catalytic particle, indicating that the formation of the T shape is not the result of catalytically guided growth (Fig. 10d).

## DISCUSSION AND SUMMARY

Catalyst-assisted growth of one-dimensional nanowires/whiskers is attributed to the vapor–liquid–solid (VLS) and vapor–solid (VS) mechanisms, in which a liquid alloy droplet composed of a metal catalyst component and a nanowire component is first formed under the reaction conditions. The metal catalyst can be rationally chosen from the phase diagram by identifying metals in which the nanowire component elements are soluble in the liquid phase but do not form solid compounds more stable than the desired nanowire phase. During growth, the catalyst droplet directs the nanowire’s growth direction and defines the diameter of the nanowire. However, our data show that nanobelts and nano-

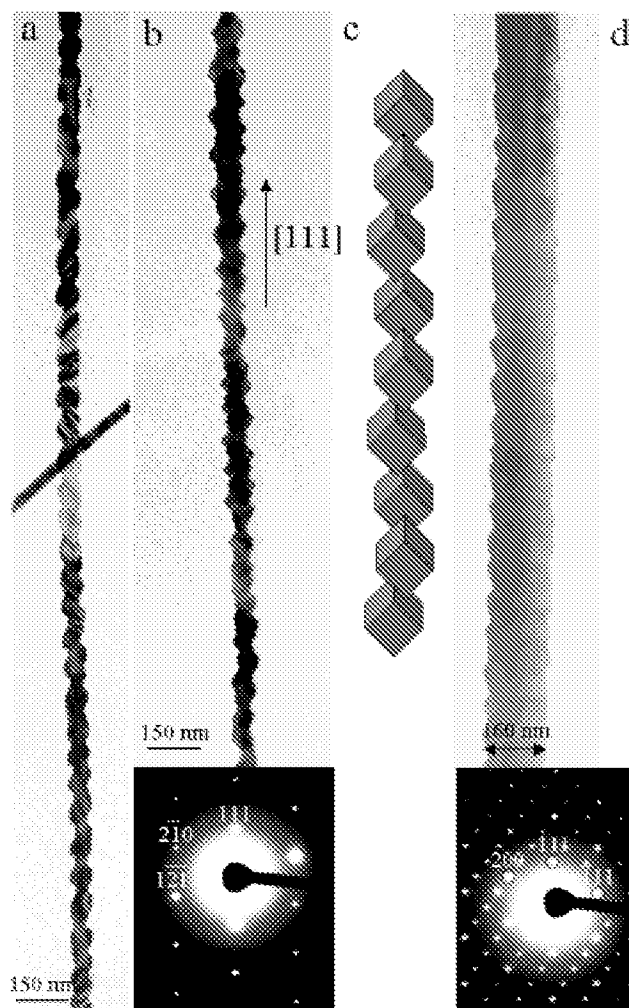


**Figure 8.** **a, b:** “Drill” shape structure of  $\text{In}_2\text{O}_3$  and the corresponding electron diffraction pattern. **c:** A model of the drill structure. **d:** A different structure of  $\text{In}_2\text{O}_3$  and the corresponding electron diffraction, displaying a superstructure.

**Table 1.** Semiconductive oxide nanobelts and their growth directions and surface planes.

Nanobelts	Crystal structure	Growth direction/plane	Top surface	Side surfaces
ZnO	Wurtzite	$[0001]$	$\pm(2\bar{1}\bar{1}0)$	$\pm(01\bar{1}0)$
ZnO	Wurtzite	$[01\bar{1}0]^*$	$\pm(2\bar{1}\bar{1}0)$	$\pm(0001)$
$\text{Ga}_2\text{O}_3$	Monoclinic	$[001]$	$\pm(100)$	$\pm(010)$
$\text{Ga}_2\text{O}_3$	Monoclinic	$[010]$	$\pm(100)$	$\pm(10\bar{1})$
$\text{SnO}_2$	Rutile	$[101]$	$\pm(10\bar{1})$	$\pm(010)$
$\text{In}_2\text{O}_3$	C-Rare earth	$[001]$	$\pm(100)$	$\pm(010)$
CdO	NaCl	$[001]$	$\pm(100)$	$\pm(010)$
$\text{PbO}_2$	Rutile	$[010]$	$\pm(201)$	$\pm(10\bar{1})$

\*The nanobelts have a single stacking fault/twin parallel to the growth direction throughout the entire length.

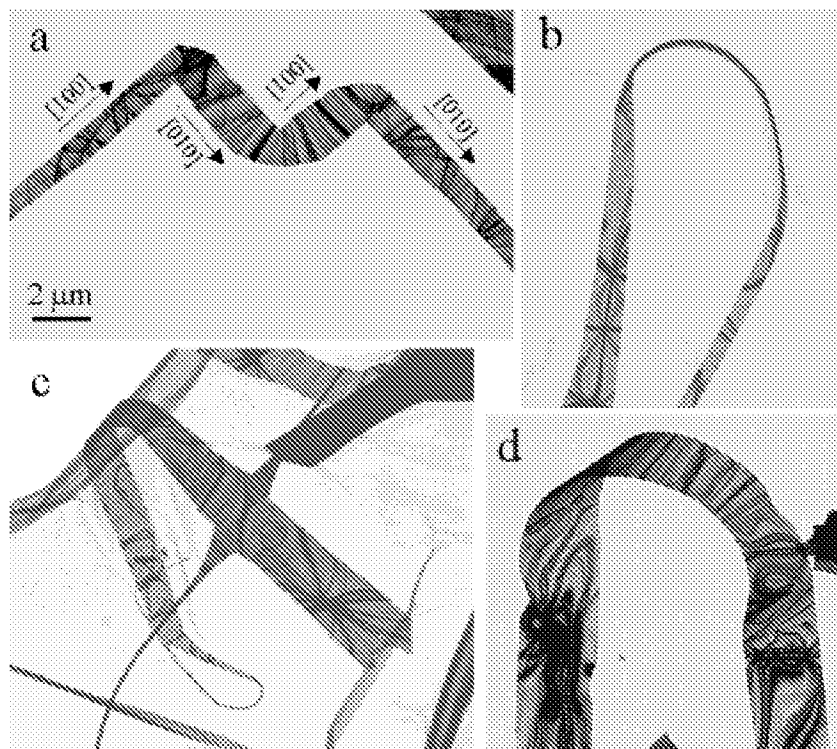


**Figure 9.** Various morphologies of CdO nanobelts and nanosheets as a result of growth kinetics.

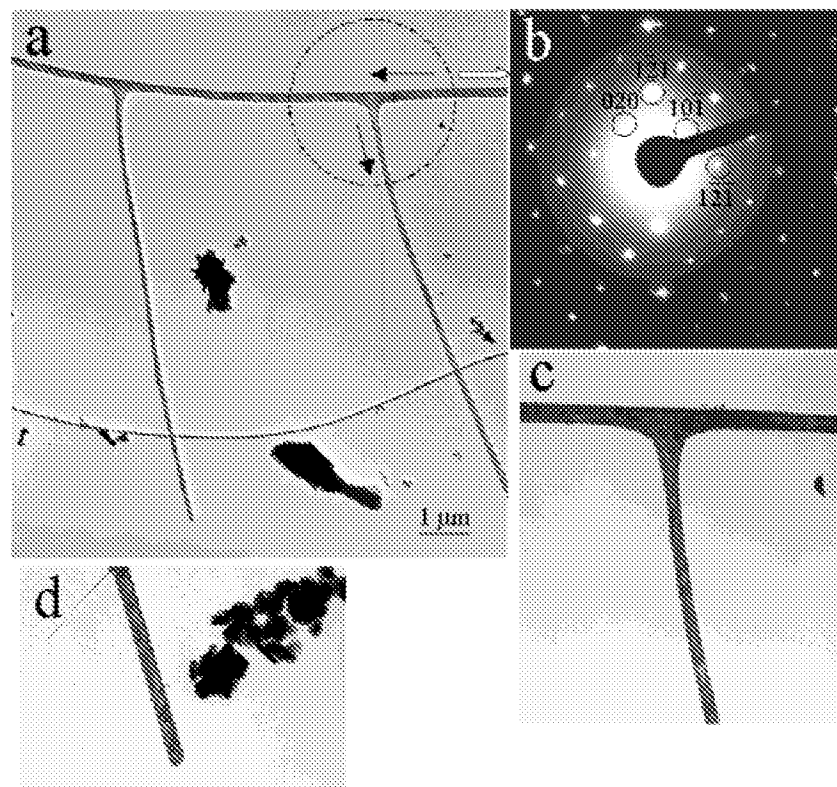


**Figure 10.** **a:** T shape structure of SnO<sub>2</sub> nanowires. **b:** The corresponding electron diffraction pattern, where the electron beam is [101]. **c, d:** Enlarged TEM images from the growth tip and the T junction of the nanowire.

wires can be obtained without the assistance of the metal catalyst, and no apparent catalyst particle presents at the end of the nanobelt or nanowire. Since the oxide nanowires or nanobelts were usually prepared by an evaporation-based synthetic method, in which only oxide vapor and solid oxide products were involved, it is likely that the growth of the oxide nanostructures was governed by a VS process. In the VS process, the oxide vapor, formed at a higher temperature region, directly deposits onto a substrate at a lower temperature region and grows into nanobelts or nanowires.

Unlike the well-developed VLS process, the detailed VS process, for example, how atoms or other building blocks can be rationally assembled into one-dimensional nanostructures with wirelike or beltlike morphologies, is still not fully understood. The role played by planar defects is still unclear, such as stacking faults and twins, because they are rarely observed in the growth products.

In this article, we presented the microstructural studies of oxide nanobelts and nanowires of ZnO, In<sub>2</sub>O<sub>3</sub>, and CdO. The planar defects and some surface morphologies observed in these systems are demonstrated. We have shown that the growth of the oxide nanostructure is governed by surface energy and growth kinetics. It appears that the growth is strongly influenced by the experimental conditions, such as temperature, temperature gradient, and gas flow rate. The formed surfaces are the low index, low energy

facets; the morphologies of the nanostructures are largely determined by the growth conditions.

## REFERENCES

---

- DAI, Z.R., PAN, Z.W. & WANG, Z.L. (2001a). Gallium oxide nanoribbons and nanosheets. *J Phys Chem B* **106**, 1274–1279.
- DAI, Z.R., PAN, Z.W. & WANG, Z.L. (2001b). Ultra-long single crystalline nanoribbon of tin oxide. *Solid State Commu* **118**, 351–354.
- DUAN, X.F., HUANG, Y., CUI, Y., WANG, J. & LIEBER, C.M. (2001). Indium phosphide nanowires as building blocks for nanoscale electronic and optoelectronic devices. *Nature* **409**, 66–69.
- GALASSO, F.S. (1970). *Structure and Properties of Inorganic Solids*. New York: Pergamon Press.
- IJIMA, S. (1991). Helical microtubules of graphitic carbon. *Nature* **354**, 56–58.
- MORALES, A.M. & LIEBER, C.M. (1998). A laser ablation method for the synthesis of crystalline semiconductor nanowires. *Science* **279**, 208–211.
- PAN, Z.W., DAI, Z.R. & WANG, Z.L. (2001a). Lead oxide nanobelts and phase transformation induced by electron beam irradiation. *Appl Phys Letts* **80**, 309–311.
- PAN, Z.W., DAI, Z.R. & WANG, Z.L. (2001b). Semiconducting oxide nanobelts. *Science* **291**, 1947–1949.
- WANG, Z.L. & KANG, Z.C. (1998). *Functional and Smart Materials—Structural Evolution and Structural Analysis*. New York: Plenum Press.